Experimental and numerical vibration correlation of pre-stressed laminated reinforced panel

Experimental and numerical vibration correlation of pre-stressed laminated reinforced panel

P.H. Cabral[1], E. Carrera[2], H.E.A.A. dos Santos[1], P.H.G. Galeb[1], A. Pagani[2], D. Peeters[3], A.P. Prado[1]

[1]Embraer S.A., São José dos Campos 12227-901, Brazil.
[2]MUL2, Department of Mechanical and Aerospace Engineering, Politecnico di Torino, Corso Duca degli Abruzzi 24, 10129 Torino, Italy.
[3]Faculty of Aerospace Engineering, Delft University of Technology, Kluyverweg 1, Delft 2629HS, the Netherlands.

Abstract: *This research work deals with the buckling load prediction of reinforced laminated composite panels of aeronautical interest. Being subjected to pure compression, these panels are characterized by stable post-buckling. Thus, the Vibration Correlation Technique (VCT) is utilized herein as an effective nondestructive means to extrapolate critical loads from free vibration measurements. A hierarchical design of experiments, making use of nested multifactors (i.e., panel replicas, test setups, and measurement repetitions), is employed to estimate components of variance. The experimental outcomes are compared with the results of an advanced finite element model with layer-wise kinematics and based on the Carrera Unified Formulation (CUF). The results show that, although obtained with a low number of tests and specimens, the VCT experiments are repeatable and provide a good validation of the numerical simulations, which are demonstrated to be accurate and reliable.*

Keywords: Vibration correlation technique; Composite stiffened panel; Layerwise models; Design of experiments.

---

1 Introduction

The natural frequencies and mode shapes of structures are functions of the equilibrium condition. Under the assumption that the vibration modes are similar to buckling ones, one can plot the relationship between the natural frequencies and the progressively higher applied (compression) loading. Thus, the predicted buckling load can be extrapolated as the load which causes zero natural frequency [1]. Based on this principle, the Vibration Correlation Technique (VCT) has been successfully applied as a nondestructuve methodology to predict the buckling loads of axially loaded columns and panels. In the ideal case of stable buckling (i.e., Euler buckling), the natural frequency squared and the compressive load are linearly dependent [2], so that:

$$\left(\frac{f}{f_0}\right)^2 + \left(\frac{P}{P_{cr}}\right) = 1 \tag{1}$$

where f is the natural frequency of the structure under load P, f_0 is the natural frequency of the unloaded structure, and P_{cr} is the critical buckling load.

Abramovich *et al.* [3] demonstrated that Eq. (1) holds for simply supported columns, whereas for other boundary conditions the straight line of the f^2 vs P graph becomes slightly curved. This is also the case, for example, of shell structures for which the VCT predicts a buckling load that is higher than the experimental one, mainly because of initial imperfections [4, 5]. For this reason, many authors have formulated more evolute formulation for the VCT-based prediction of critical loads of structures with unstable post-buckling. Souza *et al.* [6, 7], for instance, proposed a quadratic fit of the f^2 vs P curve, in the form:

$$\left(1-\frac{P}{P_{cr}}\right)^2+\left(1-\xi^2\right)\left(1-\left(\frac{f}{f_0}\right)^4\right)=1 \tag{2}$$

where, eventually, ξ represents the experimental knock-down factor.

In the present work, VCT in a shape which is similar to Eq. (2) is used for the buckling prediction of a composite stiffened panel of aeronautical relevance. Literature about VCT analysis of flat plates is less rich if compared to shells. The main reason is that plates, generally, have a stable post-buckling, which makes the problem statement simpler. Nevertheless, Lowrey [8], for example, used pseudo-random test signals and cross-correlation analysis of the determination of the dynamic-response characteristics of plate systems. Beznea and Chiric [9] carried out an experimental and numerical study on composite plates. To avoid premature out-of-plane displacements, Singhatanadgid and Sukajit [10] proposed to use tensile loading for the prediction of buckling loads of thin plates.

Particular emphasis is given herein to the study of the effects of defects, which are studied on a statistical basis, and the formulation of an advanced mathematical model for the simulation of the VCT analysis and buckling prediction of the reinforced composite panel. As far as the former topic is concerned, it shall be underlined that the uncertainty or spread in properties is usually checked at the coupon level in terms of the material characteristics. However, it is not only the spread in the material properties, but also the spread of the performance of the resulting structure that is of interest to the user. As a first step to get a grip on the uncertainty on part level, three stiffened panels were manufactured and, within the scope of the proposed research, tested for buckling under uniaxial compression. All stiffened panels were made one after the other, each placed in the autoclave separately in an attempt to have the three panels as similar as possible.

Regarding the simulation part, the finite element model used for validation and for assessing the VCT analyses is based on the Carrera Unified Formulation (CUF), see [11]. The main advantage of this method is that classical to higher-order models can be implemented with ease and in an automatic way. In fact, the governing equations and the related finite element arrays are written in terms of theory-independent fundamental nuclei (kernels) in CUF. When extended to laminated composite structures, it is therefore possible to formulate advanced models with layer-wise kinematics [12, 13, 14]. CUF-based layer-wise models are computationally efficient and provide accurate through-the-thickness stress states [15], which is of fundamental importance in the nonlinear analysis and whenever a rigorous estimation of the tangent (incremental) stiffness is required, such as in the case of VCT simulations. In this context, note that CUF was already successfully used for the vibration analysis of pre-stressed structures [16], including composite ones [17] in pre-buckling and highly post-buckling states.

This paper is organized as follows: (i) first, the test setup is described in Section 2, along with a few details about the manufactured composite panels and the design of the experiments; (ii) then, the numerical model and the governing equations in terms of CUF finite element

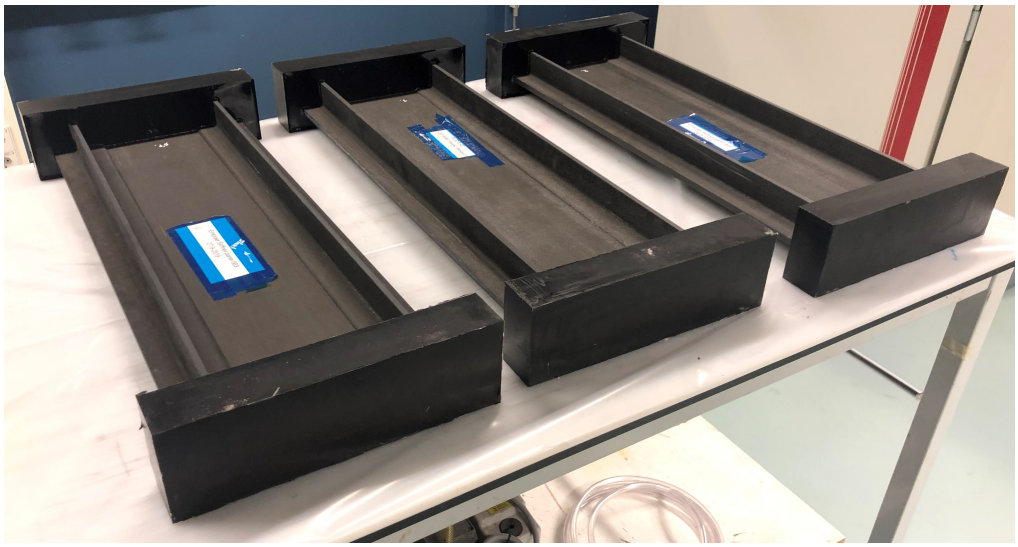

Figure 1: The three manufactured stiffened panels.

matrices for the VCT simulation are given in Section 3; (iii) next, numerical results in terms of model assessment, comparison with experiments and test data analysis are discussed in Section 4; (iv) finally, the main conclusions are outlined in Section 5.

2 Experimental setup

2.1 Manufacturing and material data

The reinforced composite panels were manufactured at the Delft Aerospace Structures and Materials Laboratory. The AS4 unidirectional prepreg employed has the following material properties: $E_1 = 119$ GPa, $E_2 = 9.8$ GPa, $E_3 = 4.67$ GPa, $\nu_{12} = 0.316$, $\nu_{13} = 0.026$, $\nu_{23} = 0.33$, $G_{12} = 4.7$ GPa, $G_{13} = G_{23} = 1.76$ GPa, and $\rho = 1580 kg/m^3$. Note that the properties in the out-of-plane directions (13 and 23) are assumed and not available from the manufacturer.

As a first step, the layers of the skin were stacked on top of each other, regularly debulking to ensure good bonding between the layers. The stiffeners were manufactured by making two parts from the same layup, again often debulking them. In detail, one of the two parts was flipped before being bent in L format to guarantee that the stringer web was symmetric, and finally the two L-parts were put back-to-back, obtaining the T-stringer. The noodle at the bottom between the two L-parts was filled up using uni-directional 0 degree material. Finally, the stiffeners were carefully placed on the panel and the stiffened composite panel was co-cured as a whole. During curing, care was taken to ensure that the pressure was evenly distributed, the stiffeners did not fall over and stayed in their intended position on the panel.

After curing, all sides of the panel were trimmed to their final dimensions. To provide the clamped boundary conditions on the short edges, the outer 50 mm were moulded in an epoxy. This epoxy was flattened afterwards to ensure the compression load is applied perfectly in line with the panel. The final dimension of the panel used for the simulation is the 'free' length: the part moulded in the epoxy is not modelled. The three finished panels are shown in Fig. 1 for the sake of completeness.

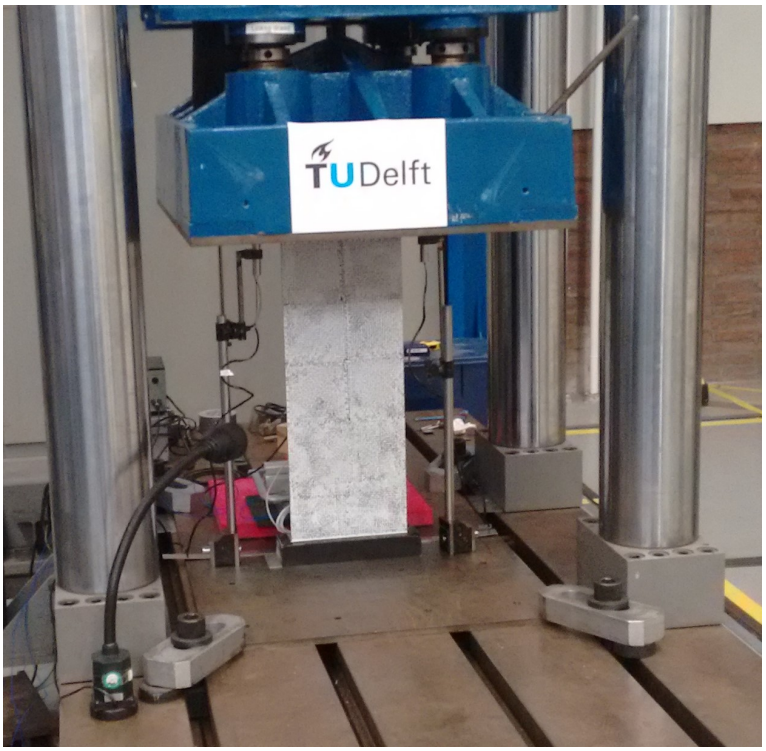

Figure 2: MTS machine at the Delft Aerospace Structures and Materials Laboratory.

2.2 Testing machine and data acquisition

The compression tests were performed using a MTS machine with a maximum force of 3500 kN and an accuracy of 1 kN. One of the panels placed in this machine is shown in Fig. 2. During the initial tests, VCT was performed with loads up to 600 kN; i.e. approximately 80% of the expected buckling load. A Polytec laser vibrometer was used for the data acquisition. A shaker was used as excitation device, using a frequency sweep between 0 and 1000 Hz. The load was gradually changed to ensure the panel does not fail due to dynamic defects. A measurement with the vibrometer was performed every 100 kN, leading to 6 measurements. The shortening was measured using 2 linear vertical displacement transducers (LVDT): one was placed on each side of the panel to ensure the panel was loaded in pure compression and no moment was induced on it.

The grid used to measure the mode shapes was 3×7. This number of grid points was chosen based on the expected buckling modes: three points in width direction were necessary to measure whether or not any torsion occurs, seven points in length direction were deemed necessary to clearly see the number of halfwaves. During the initial run, the full grid was used. In contrast, in the subsequent runs only nine points were used: the seven on the centre line in length direction, two additional left and right of the centre point. This coarser grid allowed to significantly reduce the measurement time while still being able to distinguish between the different modes.

During the final test to buckling (and failure), the laser vibrometer was removed, the LVDTs were kept in place. Additionally, three strain gauges were used: two placed back-to-back in the centre, which is the location where the buckling mode shape is expected to introduce a rotation, and one on top of the stiffener to check that the stiffener does not deform more than the panel and the load is indeed pure compression. Finally, also digital image correlation was used: the flat side of the stiffened panel was painted white and a

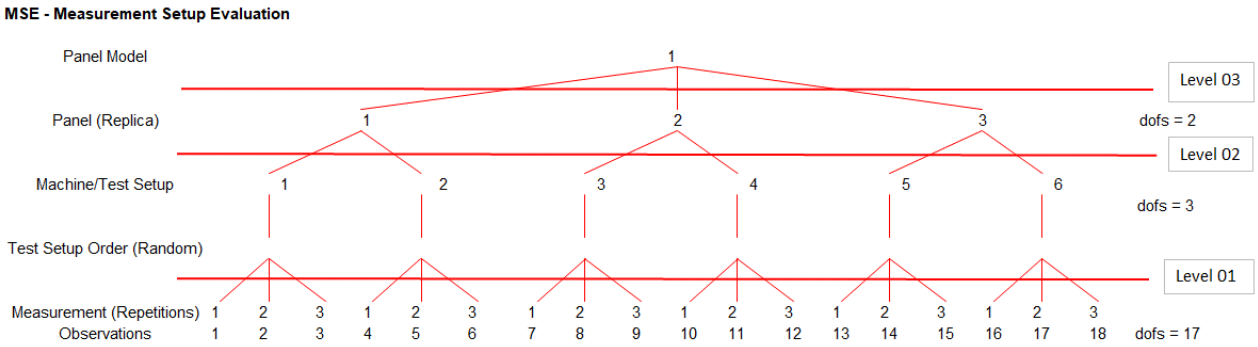

Figure 3: MSE (measurement setup evaluation) schematic design.

random speckle pattern was applied to it, to measure the full-field displacement of the panel. However, note that VCT is the main subject and detailed full-field strain evaluation is not discussed in the present study.

2.3 Measurement setup evaluation

Data from an experiment are frequently affected by more than one source of variation. This fact must be taken into account during the design of experiments and analyses of the results. According to Montgomery [18], in certain multifactor experiments the levels of one factor (e.g., factor B - or setup in our case) are similar but not identical for different levels of another factor (e.g., factor A - or panel replica in our particular case). Such an arrangement is called a nested or hierarchical design; with the levels of factor B (testing setup) nested under the levels of factor A (panel replica). Hierarchical design is an alternative experimental arrangement often employed to estimate components of variance [19].

In our experiment, there are three panel replicas that are identical panels built with the same design using the same manufacturing processes and equipment with the same batch of raw material. Each panel was fixed at the compression testing machine twice in random order and for each testing setup the panel was subjected to three cycles of compression at pre-determined loading levels. At each loading level, a set of Frequency Response Functions (FRFs) were evaluated and used to determine the changes in the panel's modal frequencies.

The objective is to investigate if the panel design behaviour is the same for each panel replica taking in account the uncertainties in the measurement system chain, such as variations that arise from panel preparation (panel adjustment and sensors and shaker positioning) at testing machine and variations that arise from repeated loading at the same panel replica. In this design of experiment, there are two testing setups for each panel replica, and three determinations of FRFs sets for each of the six different compression loading levels, from 100 to 600 kN at every 100 kN load increment. Figure 3 represents the experimental scheme described above. In this context, four FRFs peaks were monitored, where each peak is related with a vibration mode shape. By tracking the mode shapes it is possible to measure their frequency change at each loading level and extrapolate the modal and frequency change to predict the linear static buckling load in a non-destructive testing scheme.

It is worth to mention that we have adopted a screening experimental strategy where we selected the bare minimum number of tests able to furnish a quantification of the sources of variation and its magnitude involved in such arrangement and, at the same time, to keep the experimental costs as low as possible. Inevitably, some of the observed variability will be inherent in the units or items that are being measured, and some will result from the

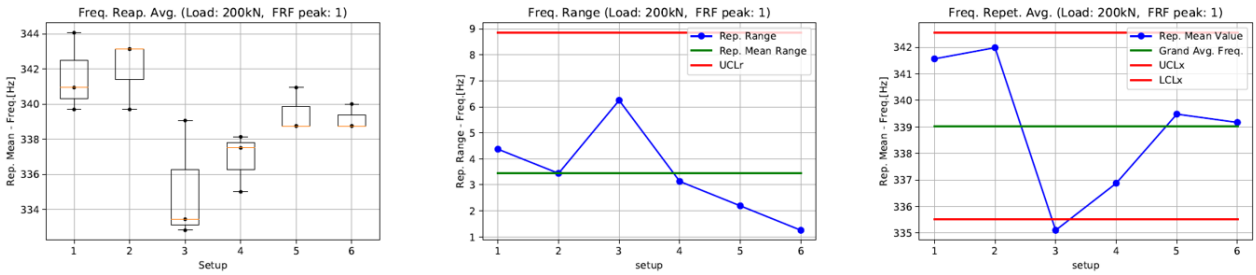

Figure 4: Repetition level boxplot, R and Mean charts for FRF peak 1 at 200 kN. The green line is the average; the read lines are the upper and lower control limits.

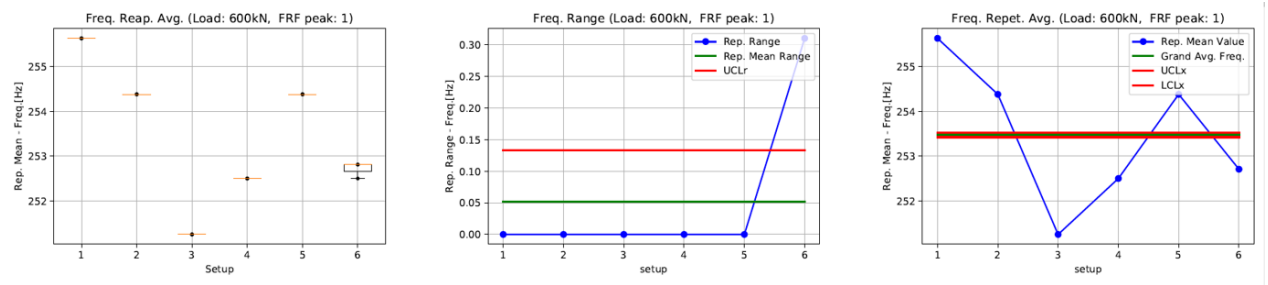

Figure 5: Repetition level boxplot, R and Mean charts for FRF peak 1 at 600 kN. The green line is the average; the read lines are the upper and lower control limits.

measurement system that is used. There may also be other factors that impact measurement system performance, such as setup or calibration activities. The purpose of our MSE (measurement setup evaluation) study is to determine how much of the total observed variability is due to the measurement chain, isolate the components of variability in the measurement system and also assess whether the experimental measurement setup is suitable for the intended application (in our case, the VCT).

2.4 Test data analysis

Figures 4 and 5 show the boxplot, the range R and the Mean charts for FRF peak 1 at 200 and 600 kN compression loads, respectively. Figure 4 shows that we have more than 5 different levels at R-chart that means an adequate measurement discrimination for a subgroup with 3 repetitions. In addition, the R-chart is within the control limits which makes possible the estimation of the natural variance of the system (the variance assigned to repetitions). On the other hand, the Xbar-chart within the control lines means that the system is not able to distinguish among setups because the natural variation of the measurement process (repetitions) has the same order of variation of the setup effects for FRFs peak 1 at 200 kN. We can interpret this result as the system ability to determine the variance of the repetitions with an adequate discrimination as well as that the effects caused by different setups are not distinguishable.

In contrast, Fig. 5 shows that we have only 2 different levels at R-chart and one point is out of the control line. As opposed to Fig. 4, we do not have an adequate discrimination and the variance estimate is not possible. However, this R-chart gives us other pieces of information. We can notice that the FRFs resolution is around 0.3 Hz. Thereby if we want to have an adequate variance estimate for the repetitions at this load level, we must increase the FRFs frequency discretization, e.g., to 0.05 Hz or even smaller frequency lines. This

also means that the experiment repeatability is higher for higher loads and consequently its variance is smaller.

3 The numerical model

3.1 Geometry and boundary conditions

Figure 6 shows the main geometrical features and the boundary conditions employed for the generation of the mathematical model. The two-stringer reinforced panel is 690 mm long and the width is $b = 270$ mm. Figure 7 shows the dimensions on the cross-section. Here, the stringer height and thickness are $h = 39.3$ mm and $t = 7.3$ mm, respectively, whereas $h_1 = 9.52$ mm and $h_2 = 3.66$ mm.

Boundary conditions are imposed on displacement components on planes perpendicular to the y-axis, as shown in Fig. 6. Two rigid bands of 50 mm each are modelled at the panel ends to simulate the real conditions resulting from the resin blocks. Note that at $y = 0$ the cross-section is free to translate, whereas a pressure is applied on the entire plane.

Figure 8 gives a pictorial view of the lamination sequences of the composite panels and the reinforcement. Note that a full layer-wise model is used in this paper. The stringer is considered as perfectly bonded to the panel, as failure considerations and stringer detachment mechanisms are not objects of the present study. Moreover, whenever possible, adjacent physical layers having the same lamination angle are studied as a single layer. This justifies the differences in the ply thickness in the figure. Although, this simplification does not affect the validity of the analysis and does not alter the capability of the proposed layer-wise model to provide high-fidelity internal stress states, which is of fundamental importance in the calculation of the geometric stiffness.

3.2 Layer-wise kinematics

Many theories of structure have been introduced in the recent past for the study of the mechanical response of laminated structures. These theories are usually divided into two categories: equivalent-single layer (ESL) and layer-wise (LW). In the case of ESL, the number of variables is independent of the number of layers. ESL theories are very attractive due to their lower computational costs and they are extensively employed by engineers to acquire

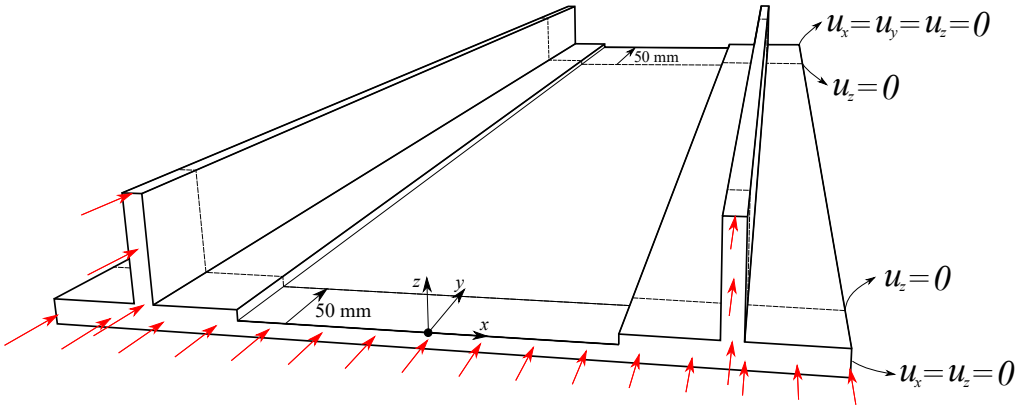

Figure 6: Main geometrical features, loadings and boundary conditions for the simulation of the reinforced composite panel.

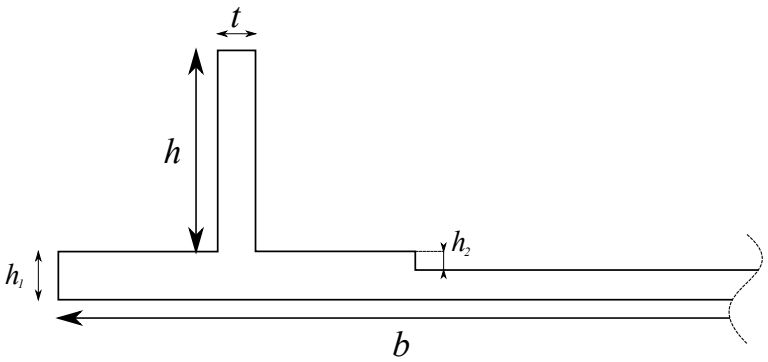

Figure 7: Detail of the panel's cross-section.

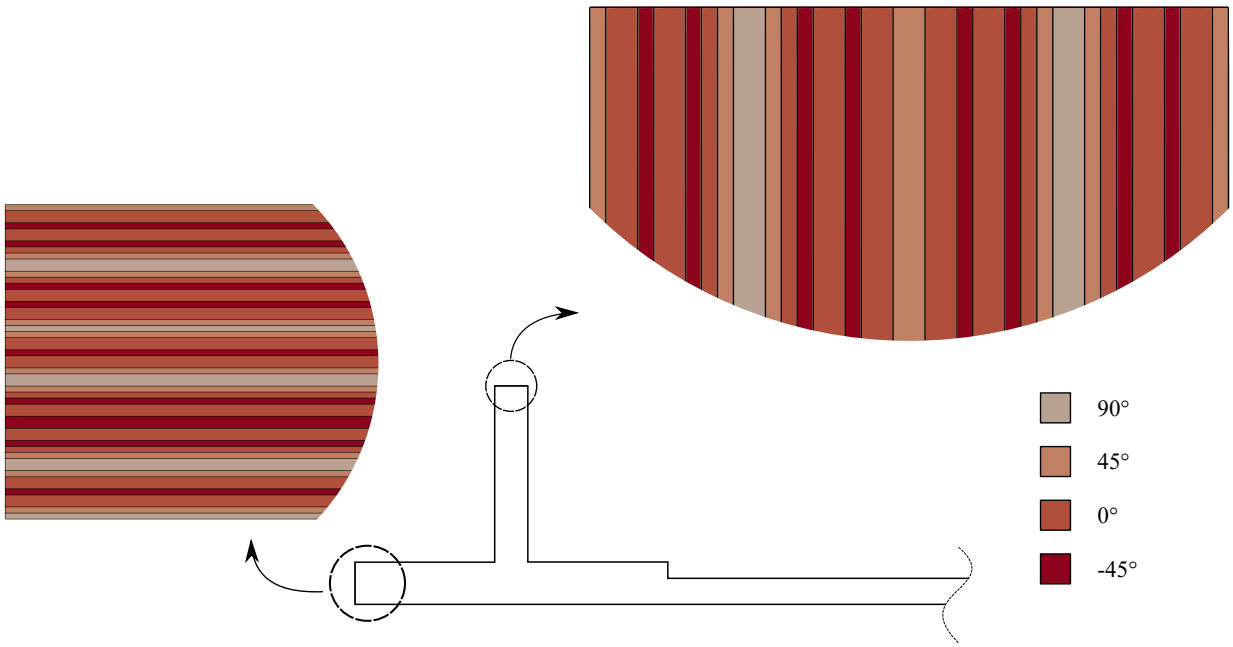

Figure 8: Stacking sequence.

information about the global response of the composite structure. However, these theories, which in most cases make use of C^1 kinematics across the stack of plies, are not suitable for providing accurate 3D stress fields at the meso-scale. In contrast, LW theories make use of independent assumptions for each layer, allowing it to capture the intralaminar deformations with higher resolution [14]. In fact, LW models are able to capture the zig-zag effect of the displacements in the thickness direction, which is strongly related to the complex distribution of transverse stresses in composite laminates, as noted by Carrera [20, 21].

In this context, a LW model has been developed for the study of the composite reinforced panel. The LW model -subject of the present study- has been obtained in the framework of the Carrera Unified Formulation (CUF), which allows to generate theories of structures in a systematic manner. Briefly, as the length of the panel is higher than the cross-section dimensions, one may assume the 3D displacement field of the k^{th} ply as the generic expansion of the *generalized* displacements $\boldsymbol{u}^k_\tau(y)$, which are functions of the coordinate y laying along the main structural dimension; i.e.,

$$\boldsymbol{u}^k(x,y,z) = F_\tau(x,z)\boldsymbol{u}^k_\tau(y), \qquad \tau = 1,2,....,M \tag{3}$$

where F_τ represent functions of the coordinates x and z on the cross-section and determine the class of the CUF model, M stands for the number of the terms used in the expansion, and the repeated subscript τ indicates summation.

Lagrange Expansions (LE) CUF models were introduced by Carrera and Petrolo [22] and are based on the use of Lagrange polynomials as expansion functions F_τ of the cross-sectional coordinates. The advantages of using Lagrange polynomials at the layer scale to develop LW models are many:

- the degrees of freedom have a clear physical meaning as they are pure displacements;
- as a consequence, the resulting finite element arrays are well conditioned;
- the displacement compatibility at the layer interface can be imposed automatically, without the use of artifices.

For the sake of completeness, the explicit expressions of a F_τ nine-node quadratic expansion (hereinafter denoted to as L9) are reported in the following:

$$\begin{aligned}
F_\tau &= \tfrac{1}{4}(r^2 + rr_\tau)(s^2 + ss_\tau) && \tau = 1,3,5,7 \\
F_\tau &= \tfrac{1}{2}s_\tau^2(s^2 - ss_\tau)(1-r^2) + \tfrac{1}{2}r_\tau^2(r^2 - rr_\tau)(1-s^2) && \tau = 2,4,6,8 \\
F_\tau &= (1-r^2)(1-s^2) && \tau = 9
\end{aligned} \tag{4}$$

where r and s are the coordinates of the natural plane [-1,1]×[-1,1] and r_τ and s_τ are the position of the nodes. L9 approximations are of particular interest for the present research, because they are used here to approximate the ply kinematics. These LW models have been demonstrated, in fact, to be effective for the approximation of global response as well as of the internal stress state of laminates, see [15].

3.3 Finite element approximation

Given the approximation of Eq. (3), the generalized displacements can be approximated along the y-axis by discretizing the 1D support with finite elements to have:

$$\boldsymbol{u}^k_\tau(y) = N_i(y)\ \boldsymbol{q}^k_{\tau i}, \qquad i = 1,2,...,n \tag{5}$$

In Eq. (5), i stands for summation and the generalized displacements are described as a function of the unknown nodal vector, $\boldsymbol{q}_{\tau i}^k$, and the 1D shape functions, N_i. When using Lagrangian shape functions, as in the current work, n stands for the number of nodes per element. The main advantage of using a compact notation as in Eqs. (3) and (5) is that the governing equations and the finite element arrays can be formulated in a unified and hierarchical manner, which is affected neither by the choice of the theory of structure, represented by F_τ, nor by the FE shape functions N_i.

The governing equations describing the free vibration around trivial equilibrium states can be formulated via the principle of virtual work, which holds:

$$\delta L_{\text{int}} - \delta L_{\text{ine}} = 0 \tag{6}$$

where L_{int} stands for the strain energy, L_{ine} is the work of the inertial loads, and δ represents the virtual variation. As in this work we are interested to vibration of structures subjected to initial displacements and pre-stress, Eq. (6) must be linearized around non-trivial equilibrium states. The linearization of the virtual variation of the internal strain energy holds:

$$\delta^2 L_{\text{int}} = \int_l \int_\Omega \delta \left(\delta \boldsymbol{\epsilon}^T \boldsymbol{\sigma} \, \mathrm{d}x \mathrm{d}z \right) \, \mathrm{d}y \tag{7}$$

where l is the dimension of the panel along the y-axis, Ω is the cross-section, and $\boldsymbol{\epsilon}$ and $\boldsymbol{\sigma}$ represent the strain and displacement vectors. Now, by using constitutive laws and geometric relations, Eq. (7) can be expressed in terms of displacements. Thus, by substituting CUF (Eq. (3)), the finite element approximation (Eq. (5)), and after opportune expansion of the indexes τ and i, $\delta^2 L_{\text{int}}$ can be written in terms of the tangent stiffness matrix $\mathbf{K}_T$:

$$\delta^2 L_{\text{int}} = \left(\delta \boldsymbol{q}^k \right)^T \, \mathbf{K}_T^k \, \delta \boldsymbol{q}^k \tag{8}$$

Note that the tangent stiffness is expressed at the layer scale in this work and, thanks to CUF, can be generated for any structural finite element, given F_τ and N_i. For more details, see [23].

In the case of small displacements and linear pre-buckling, the tangent stiffness can be approximated as the sum of the linear stiffness ($\mathbf{K}_0$) and the geometric (pre-stress) contribution ($\mathbf{K}_\sigma$) [16].

$$\mathbf{K}_T^k \approx \mathbf{K}_0^k + \mathbf{K}_\sigma^k \tag{9}$$

Once the tangent stiffness is obtained for each ply of the composite reinforced laminate, a LW assembly procedure is performed according to [24, 25] to give the global tangent stiffness matrix $\mathbf{K}_T$. Next, by considering harmonic motion around quasi-static equilibrium states, and by assuming a linear mass matrix $\mathbf{M}$, Eq. (6) assumes the form of a linear eigenvalue problem:

$$\left(\mathbf{K}_T - \omega^2 \mathbf{M} \right) \mathbf{q} = 0 \tag{10}$$

where ω is a natural period and $\mathbf{q}$ the related amplitude eigenvector.

4 Results

4.1 Model verification and internal stress state

The panels were sized in terms of lamination parameters using an optimisation technique that resulted in a final design with many active constraints, such as multiple buckling modes

Table 1: Results from compression static test in terms of shortening and applied compression loading and comparison with simulations.

	Shortening [mm]	Loading [N]	Compression modulus [kN/mm]
Experiments			
Panel 1	2.61	599'975	229.9
Panel 2	2.61	599'823	229.8
Panel 3	2.61	599'976	229.9
Simulations			
Nastran model	2.41	600'000	249.0
Present CUF model	2.41	600'000	249.0

that occurred within less than 10% of the lowest buckling load. Furthermore, the panels were designed to fail (using open-hole compression allowables) at the buckling load, by using the slice and swap method [26]. In addition to the lamination parameters, the optimisation changed the width, height and thickness of the stiffener and the thickness of the panel. Due to the extreme design requirements, a preliminary static test was performed for validation purpose and the panels were loaded in compression in the geometrically linear regime, before any buckling and failure mechanisms are activated.

Table 1 shows the results from these static compression tests. The results demonstrate a very little scatter between the different panels and a good correlation with the numerical models. Note that the Nastran model was built by using 2D CQUAD elements, based on a first-order shear approximation theory (FSDT) and homogenized properties across the thickness. As demonstrated in the previous literature, this model is appropriate for linear static considerations, but should be avoided whenever the evaluation of internal stress state is of fundamental importance, e.g. for failure consideration and buckling, see [15, 27].

In contrast, the proposed LW model makes use of CUF fundamental nuclei to build an advanced-kinematics theory based on multiple L9 subdomain across the panel cross-section. The LW model has independent unknowns for each single layer of the lamination for a total of 715'365 degrees of freedom. Although the compression stiffness is the same as the one provided by the Nastran model and well correlated to the experimental results (see Table 1), the proposed LW model is able to describe accurately the internal three-dimensional stress state within the entire structural domain. For representative purpose, Fig. 9 shows some important in-plane and out-of-plane distributions of stresses within one quarter of the composite panel, subjected to a generic compression pressure of 1 MPa.

4.2 Stability analysis vs VCT

Because the panels were designed to fail and buckle at roughly the same load, doing repeating buckling tests was not possible. To overcome this problem first vibrational correlation testing (VCT) was performed, followed by tests to failure using digital image correlation (DIC). Failure tests, however, will be discussed in a companion paper and are not part of the discussion herein.

As a preliminary analysis, Table 2 shows the important natural frequencies and critical linearized buckling loads according to the proposed numerical model. For completeness rea-

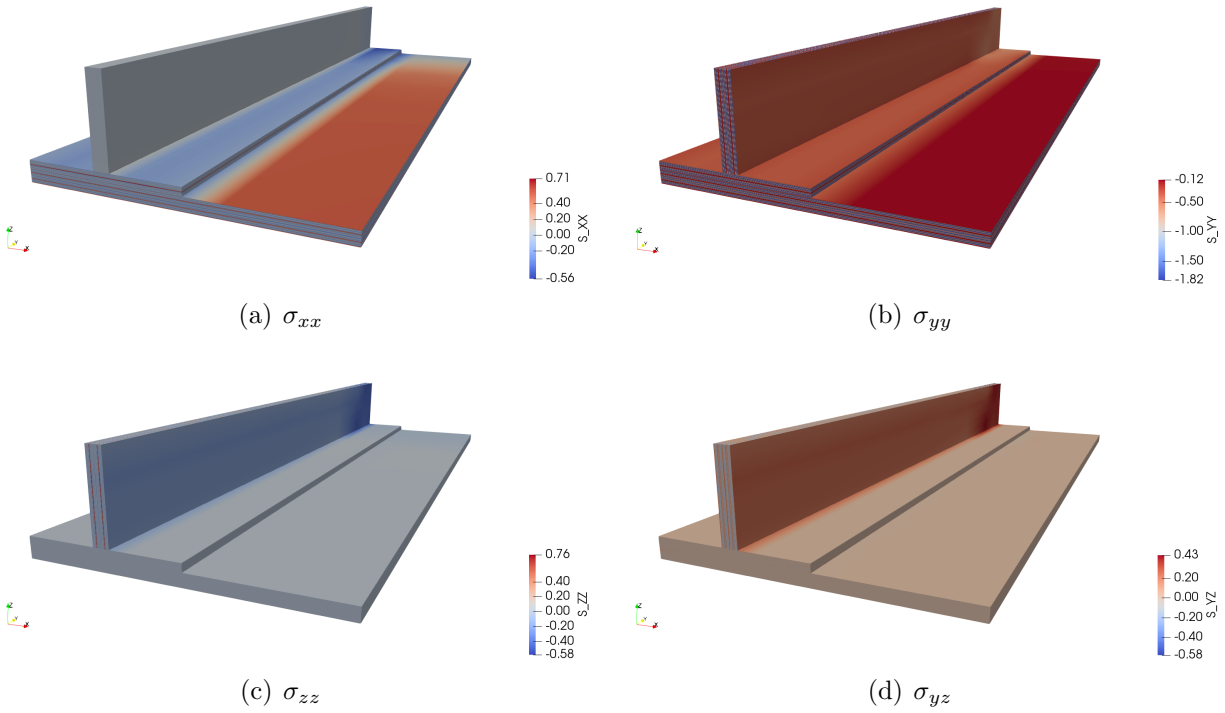

(a) σ_{xx} (b) σ_{yy}

(c) σ_{zz} (d) σ_{yz}

Figure 9: Internal stress state within one quarter of the reinforced composite panel subjected to a representative compression pressure of 1 MPa. Results are in MPa.

Table 2: First four natural frequencies and linearized buckling loads according to the present CUF-based LW model of the reinforced composite panel.

Mode	Natural frequency [Hz]	Buckling load [kN]
1	368	739
2	476	745
3	562	809
4	663	830

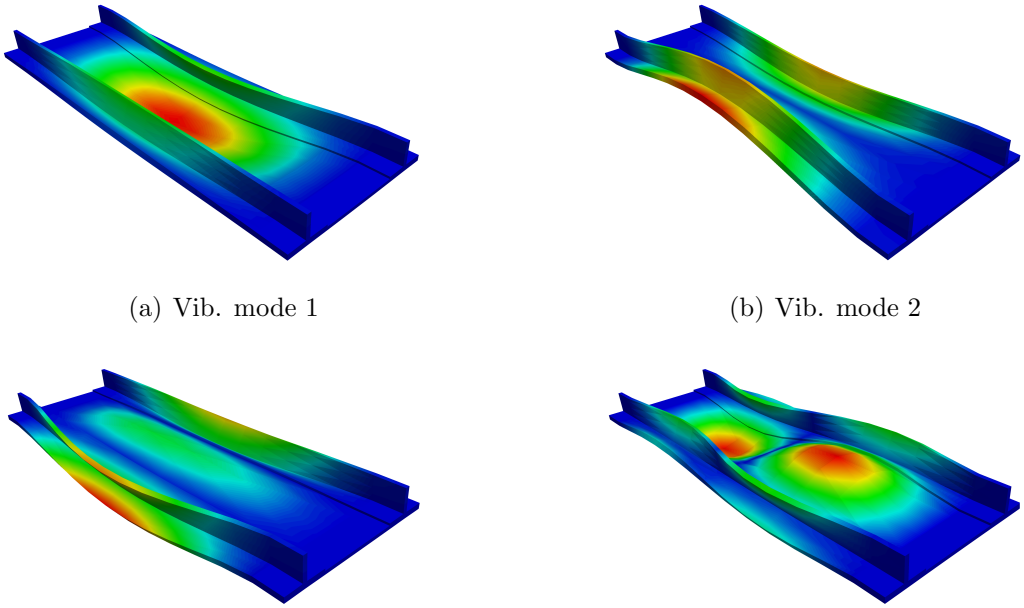

(a) Vib. mode 1 (b) Vib. mode 2

(c) Vib. mode 3 (d) Vib. mode 4

Figure 10: Free vibration modes of the unloaded reinforced composite panel according to the present CUF-based LW model.

sons, Fig.s 10 and 11 show the respective mode shapes. Note that, as per design requirements, the buckling loads are close each other. This aspect makes the simulation and the experimental evaluations very demanding. Also, justification on the use of VCT for the proposed problem comes from the comparison between free vibration mode shape number 4 and the first buckling mode.

During the VCT the load was increased in steps of roughly 13.5% up to 80% of the failure load to ensure the panels were not damaged during these tests. As discussed in Section 2, this test was repeated three times before placing a different panel in the machine to check the variability due to repeating the tests. Each panel was placed twice in the machine to check the variability due to the setup of the test. Finally, by having three panels, the influence of the replicas could be analysed. The mean values from the VCT measurements are summarized in Table 3 and the results are compared with those coming from simulation. Generally speaking, the comparison is acceptable. The slight differences will not affect our conclusions.

Results of the VCT are shown in graphical form in Fig. 12a, where the confidence interval of the measured data is also depicted. It is clear that there is very little scatter between the repetitions, the test setup and even the different panels. Interestingly, from Fig. 12a, it is evident that the confidence interval of the measured data becomes narrow for higher compression loadings. This aspect confirms that uncertainty and measurement errors become negligible when internal stress state is higher, see Section 2.4.

From the failure tests, the buckling load can clearly be read from the load-displacement diagram (not given here). This kink was at a load of 739.9, 740.3, and 738.0 kN for the three panels. Figure 12b shows the dependence of the natural frequencies squared versus the compression load. The quadratic fit of the measured vibrations allow the estimation of the critical load ($P_{VCT} = 820$ kN). As summarized in Table 4, the load estimated by VCT shows a knock-down factor of 10%, whereas the proposed FEM model is perfectly able to predict the structural stiffness loss close to the experimental buckling load ($P_{exp} = 739$ kN).

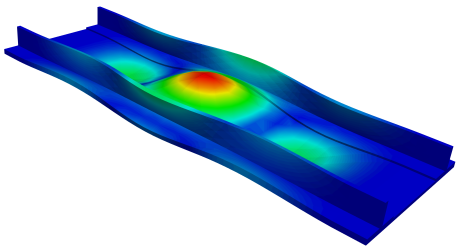

(a) Buck. mode 1

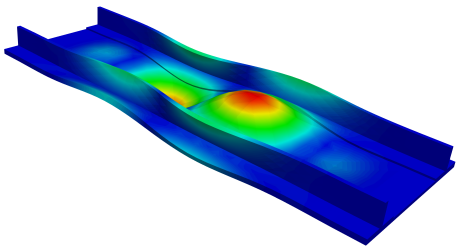

(b) Buck. mode 2

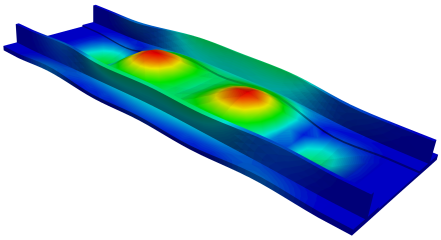

(c) Buck. mode 3

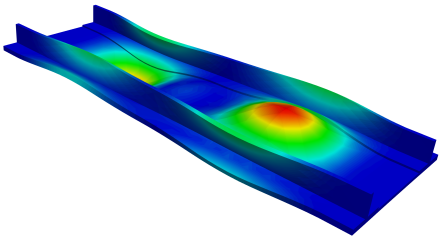

(d) Buck. mode 4

Figure 11: Buckling modes of the reinforced composite panel according to the present CUF-based LW model.

Table 3: Free vibration analysis of the composite reinforced panel subjected to compression. Comparison between the proposed CUF-based LW model and experiments.

Load [kN]	f_1 [Hz]		f_2 [Hz]		f_3 [Hz]		f_4 [Hz]	
	CUF	Exp.	CUF	Exp.	CUF	Exp.	CUF	Exp.
100	349	348	462	459	550	555	622	-
200	330	339	447	457	537	553	578	-
300	308	324	431	449	523	546	532	-
400	284	304	415	436	513	535	476	514
500	258	281	398	420	499	522	414	462
600	225	253	381	407	487	505	336	394

Table 4: Measured buckling load and comparison between VCT and CUF simulation.

	Buckling load [kN]			Error % - ref. Exp. Mean
	Panel 1	Panel 2	Panel 3	
Experimental	739.9	740.3	738.0	-
CUF model		739.0		0.00
VCT		820.0		10.0

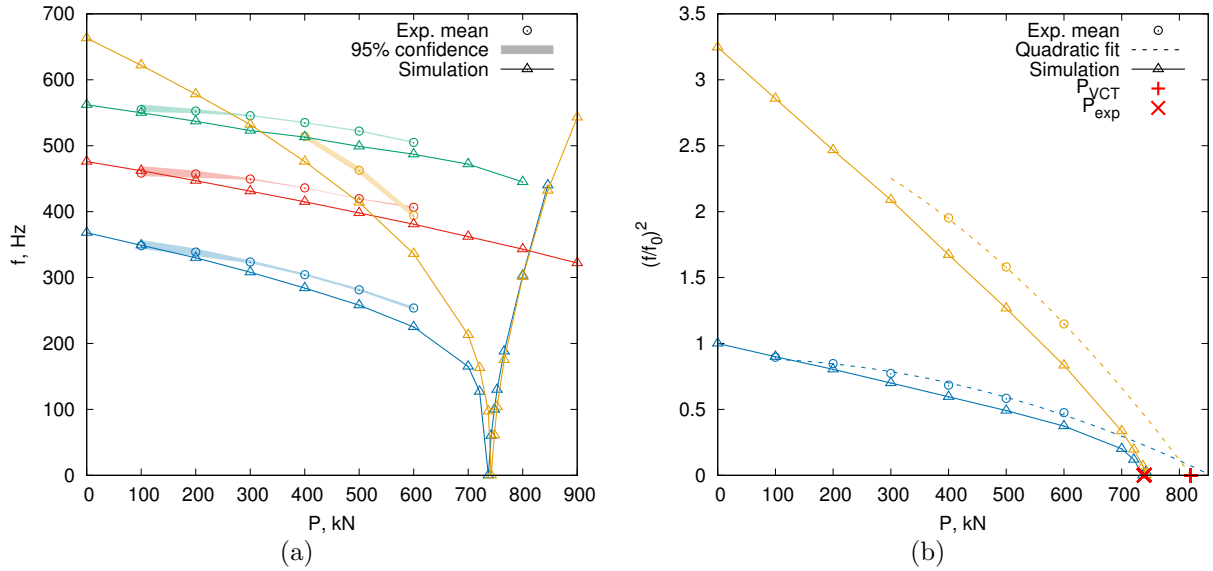

Figure 12: Vibration correlation of the first four natural mode shapes from experiments and simulation (a) and prediction of the critical load (b). $P_{VCT} = 820$ kN is the critical load extrapolated from a quadratic fit of the VCT curves. In contrast, $P_{exp} = 739$ kN is the experimental failure load. Mode 1 is shown in blue, mode 2 in red, mode 3 in green, and mode 4 in yellow.

5 Conclusions

VCT buckling load predictions of reinforced composite panels have been investigated by experiments and simulation. Since a hierarchical design of experiments has been used, the test successfully have provided us with a ballpark estimate about the components of variance present in this VCT. The results have been obtained with a low number of tests and specimens bringing the valuable information about how repeatable is the experiment and how reproducible are the panels' manufacturing process. With this information we can expand our experimental configuration in order to improve the standard variation estimates and also include other important factors such as different batches and parts suppliers, for example.

In this context, when accurate and reliable, simulation can play a fundamental role for the correlation of the experimental results and as a companion tool. This is the case indeed of the numerical model implemented in this paper, which is based on the Carrera Unified Formulation (CUF). CUF makes use of theory-independent kernels for the implementation of low- to high-order finite elements. Thus, layer-wise models of composite laminates can be formulated with ease. The use of layer-wise models able to correctly describe the internal stress state of pre-stressed structure vibrating is of paramount importance for the problem under consideration. As a matter of fact, the proposed CUF-based model of the reinforced panel are in agreement with the experimental data and gives a perfect prediction of the buckling load.

References

[1] J. Singer, J. Arbocz, and T. Weller. *Buckling experiments, shells, built-up structures, composites and additional topics*, volume 2. John Wiley & Sons, 2002.

[2] L.N. Virgin and R.H. Plaut. Effect of axial load on forced vibrations of beams. *Journal of Sound and Vibration*, 168(3):395–405, dec 1993.

[3] H. Abramovich, D. Govich, and A. Grunwald. Buckling prediction of panels using the vibration correlation technique. *Progress in Aerospace Sciences*, 78:62–73, 2015.

[4] A. Rosen and J. Singer. Effect of axisymmetric imperfections on the vibrations of cylindrical shells under axial compression. *AIAA Journal*, 12(7):995–999, jul 1974.

[5] J. Singer and J. Prucz. Influence of initial geometrical imperfections on vibrations of axially compressed stiffened cylindrical shells. *Journal of Sound and Vibration*, 80(1):117–143, jan 1982.

[6] M.A. Souza, W.C. Fok, and A.C. Walker. Review of experimental techniques for thin-walled structures liable to buckling, Part I - neutral and unstable buckling. *Experimental Techniques*, 7(9):21–25, sep 1983.

[7] M.A. Souza, W.C. Fok, and A.C. Walker. Review of experimental techniques for thin-walled structures liable to buckling, Part II - stable buckling. *Experimental Techniques*, 7(10):36–39, oct 1983.

[8] M.J. Lowrey. Use of correlation techniques in vibration studies of plate systems. *Experimental Mechanics*, 15(12):476–481, dec 1975.

[9] E.-F. Beznea and I. Chiric. Buckling and post-buckling analysis of composite plates. In *Advances in Composite Materials - Ecodesign and Analysis*. InTech, mar 2011.

[10] P Singhatanadgid and P. Sukajit. Determination of buckling load of rectangular plates using measured vibration data. In Xiaoyuan He, Huimin Xie, and YiLan Kang, editors, *ICEM 2008: International Conference on Experimental Mechanics 2008*. SPIE, nov 2008.

[11] E. Carrera, M. Cinefra, M. Petrolo, and E. Zappino. *Finite Element Analysis of Structures through Unified Formulation*. John Wiley & Sons, Chichester, West Sussex, UK, 2014.

[12] E. Carrera and M. Petrolo. Refined one-dimensional formulations for laminated structure analysis. *AIAA Journal*, 50(1):176–189, 2012.

[13] A. Pagani, A.G. de Miguel, M. Petrolo, and E. Carrera. Analysis of laminated beams via unified formulation and Legendre polynomial expansions. *Composite Structures*, 156:78–92, nov 2016.

[14] A.G. de Miguel, A. Pagani, and E. Carrera. Free-edge stress fields in generic laminated composites via higher-order kinematics. *Composites Part B: Engineering*, 168:375–386, 2019.

[15] A. G. de Miguel, I. Kaleel, M. H. Nagaraj, A. Pagani, M. Petrolo, and E. Carrera. Accurate evaluation of failure indices of composite layered structures via various fe models. *Composites Science and Technology*, 167:174–189, 2018.

[16] A. Pagani, R. Augello, and E. Carrera. Frequency and mode change in the large deflection and post-buckling of compact and thin-walled beams. *Journal of Sound and Vibration*, 432:88–104, 2018.

[17] E. Carrera, A. Pagani, and R. Augello. Effect of large displacements on the linearized vibration of composite beams. *International Journal of Non-Linear Mechanics*, 120:103390, apr 2020.

[18] D. C. Montgomery. *Design and Analysis of Experiments*. Wiley, 1984.

[19] G. E. P. Box, J. S. Hunter, and W. G. Hunter. *Statistics for Experimenters - Design, Innovation, and Discovery*. Wiley, 2005.

[20] E. Carrera. C^0 Reissner–Mindlin multilayered plate elements including zig-zag and interlaminar stress continuity. *International Journal for Numerical Methods in Engineering*, 39(11):1797–1820, 1996.

[21] E. Carrera. Historical review of zig-zag theories for multilayered plates and shells. *Applied Mechanics Reviews*, 56(3):287–308, 2003.

[22] E. Carrera and M. Petrolo. Refined beam elements with only displacement variables and plate/shell capabilities. *Meccanica*, 47(3):537–556, 2012.

[23] A. Pagani and E. Carrera. Unified formulation of geometrically nonlinear refined beam theories. *Mechanics of Advanced Materials and Structures*, 25(1):15–31, 2018.

[24] J N Reddy. An evaluation of equivalent-single-layer and layerwise theories of composite laminates. *Composite Structures*, 25:21–35, 1993.

[25] E Carrera. Multilayered shell theories accounting for layerwise mixed description, part 1: governing equations. *AIAA Journal*, 37(9):1107–1116, 1999.

[26] G. H. C. Silva, A. P. do Prado, P. H. Cabral, R. De Breuker, and J. K. S. Dillinger. Tailoring of a composite regional jet wing using the slice and swap method. *Journal of Aircraft*, 56(3):990–1004, 2018.

[27] E. Carrera, A. G. de Miguel, M. Filippi, I. Kaleel, A. Pagani, M. Petrolo, and E. Zappino. Global-local plug-in for high-fidelity composite stress analysis in femap/nx nastran. *Mechanics of Advanced Materials and Structures*. DOI: 10.1080/15376494.2019.1655689.